Modeling and Control of Periodic Humanoid Balance using the Linear Biped Model

Benjamin Stephens
Carnegie Mellon University
Pittsburgh, PA 15213, USA
Email: bstephens@cmu.edu

Christopher Atkeson
Carnegie Mellon University
Pittsburgh, PA 15213, USA
Email: cga@cmu.edu

***Abstract*—We present work on compliant control of dynamic humanoid balance and walking. We use the Linear Biped Model (LiBM) to model the dynamics of balance on two feet. To achieve periodic motion, as in walking, we derive an orbital energy controller for this model. We also present our methods for applying this control to a torque-controlled humanoid robot, which include estimating the center of mass state and generating feed-forward torque commands.**

I. Introduction

Humanoid robots are complex systems that are often studied using simple models. One such model is the *Linear Inverted Pendulum Model* (LIPM) [1]. Often, this model is used in combination with desired foot trajectories. A trajectory for the center of mass is created so that the center of pressure, or zero moment point, is always within the base of support. Rather than following pre-determined trajectories, we would like to utilize reactive controllers that stabilize the system from large and unknown perturbations.

We develop an extension of the LIPM, which we call the "Linear Biped Model" (LiBM) that describes the dynamics of having two legs and feet, shown in Figure 1. During single support, the dynamics are equivalent to a LIPM. During double support, however, the dynamics are described by two superimposed LIPMs. We present a controller that regulates periodic motion and is inspired by the concept of orbital energy [2]. An analytic controller for our simple model is derived that can achieve a desired energy level. The concept of orbital energy allows us to control periodic motion without using an internal clock.

The Linear Biped Model is used for controlling our torque-controlled humanoid robot. It is very useful because it approximates dynamic motion and ground reaction forces. We use the torques and forces predicted by the simplified model as feed-forward controls. The linear model is also used for improved motion estimation by combining various sensor measurements in a Kalman Filter. Finally, this biped model can be used to make quick decisions about stepping to recover balance as well as planning high-level walking trajectories.

This paper is outlined as follows. First, in Section II, we describe the Linear Biped Model and derive the linear dynamics. In Section III, we derive the orbital energy controller for coronal balance. We describe how a stepping controller can be written for the Linear Biped Model in IV. Then we focus on applying this model to control of our humanoid robot in V.

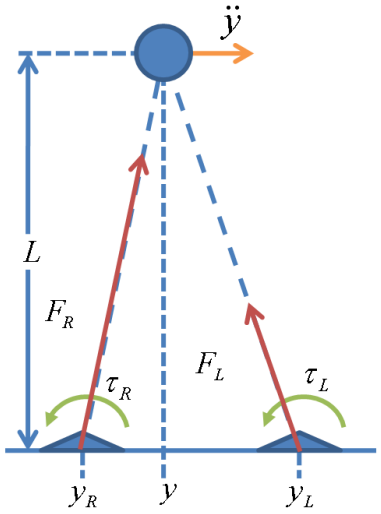

Fig. 1. The Linear Biped Model consists of two superimposed Linear Inverted Pendulum Models. It can be used for modeling, estimation and control of biped systems, such as a humanoid robot.

A. Related Work

Simple models have been widely used for control and estimation of humanoid locomotion. The LIPM has been used in combination with a model-predictive controller called "preview control" [3]. Footstep planning for the ASIMO robot [4] was achieved by ignoring much of the robot dynamics and balance control, considering only a fixed set of foot placements at each step and searching over a fixed horizon.

Many researchers have begun to focus on biped balance control. Standing dynamic balance of humanoids has been studied using simple models [5] [6] [7], integral control [8], optimization [9], and nonlinear computed torque techniques [10] [11]. Stepping has also been studied using simple models [12], reinforcement learning [13], and manifold learning [14]. In addition, the graphics community has used momentum-based techniques [15] to optimize motions for balance and stepping based on motion capture data [16].

The author has previously investigated control of standing sagittal balance [6] using simple models. We have also con-

sidered ankle torque and foot placement control of a compass model in the lateral (coronal) plane [17]. The model presented in this paper is also intended for studying balance in the coronal plane. Often, motion in this plane is periodic, as during walking. From studies of passive dynamic walking, it is shown that lateral motion is unstable, but can be stabilized by suitable control [18].

II. Linear Biped Model

For legged robots, balance is determined by the motion of the center of mass relative to the base of support. For biped robots, the base of support changes depending on whether there are one or two feet on the ground. We define a simple model that takes into account the two feet of the robot, shown in Figure 1, called the Linear Biped Model (LiBM). Like the LIPM, this model maintains a constant height above the ground, $z = L$. The dynamics vary continuously through single and double support phases. During single support, the dynamics are equivalent to the LIPM,

$$\ddot{y} = \frac{\tau}{mL} + \frac{g}{L}y \tag{1}$$

However, during double support, the dynamics are two superimposed LIPMs,

$$\ddot{y} = \frac{\tau_L + \tau_R}{mL} + \frac{g}{L}\omega_L\left(\tilde{y} - y_L\right) + \frac{g}{L}\omega_R\left(\tilde{y} - y_R\right) \tag{2}$$

where y_L and y_R are the locations of the two feet and $\tilde{y} = y - \frac{1}{2}(y_L + y_R)$ is the distance from halfway between the two feet. The two stance weights, ω_L and ω_R, vary continuously and satisfy $\omega_R + \omega_L = 1$. The complete state of the planar model is given by

$$X = \begin{pmatrix} y \\ \dot{y} \\ y_L \\ y_R \end{pmatrix} \tag{3}$$

We define a double support region, shown in Figure 2, as a fraction, γ, called the *double support ratio*, of the distance between the two feet. As the stance width changes, so does the width of the double support region. The intuition behind this is that the legs have limited length and will come off the ground at roughly the same place. This greatly simplifies the transition between phases, which we can describe using the stance weights,

$$\omega_L = \begin{cases} 1 & , \quad \tilde{y} \geq \gamma W \\ \frac{\gamma W + \tilde{y}}{2\gamma W} & , \quad |\tilde{y}| < \gamma W \\ 0 & , \quad \tilde{y} \leq -\gamma W \end{cases} \tag{4}$$

where $W = \frac{1}{2}(y_L - y_R)$ is half the stance width. The other weight is found simply by $\omega_R = 1 - \omega_L$. Because of this, Eq.(2) can be simplified to

$$\ddot{y} = \frac{\tau_L + \tau_R}{mL} - \frac{g}{L}\alpha y \tag{5}$$

where

$$\alpha = \frac{1-\gamma}{\gamma} \geq 0 \tag{6}$$

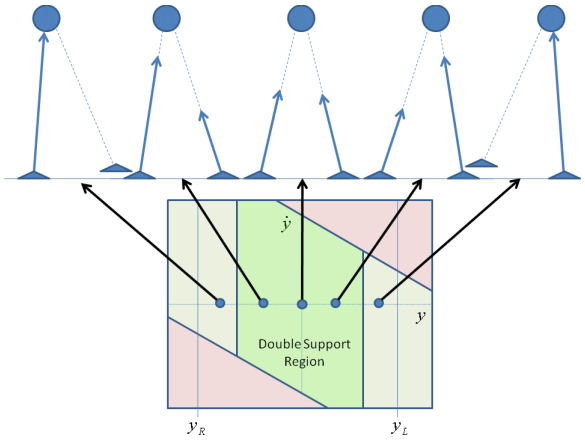

Fig. 2. The double support region is defined in the phase space of the center of mass.

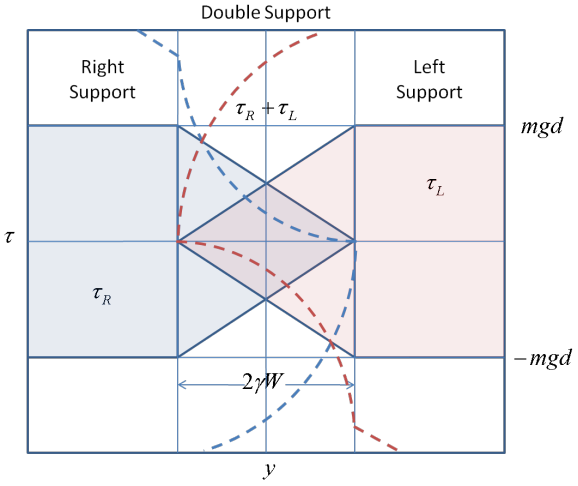

Fig. 3. The torque limits defined by the LiBM during different support phases. The solid lines are due to the center of pressure constraint and the dashed lines are due to the friction cone.

The result is a spring-mass system, or a simple harmonic oscillator, that is stable for any initial state that satisfies

$$y_L + d \geq \dot{y}\sqrt{\frac{L}{g}} + y \geq y_R - d \tag{7}$$

where d is half the width of the foot and the bounds represent the edges of the base of support.

One of the benefits of this model is we can also determine the forces on the feet,

$$\begin{pmatrix} F_{LY} \\ F_{LZ} \\ M_{LX} \end{pmatrix} = \begin{pmatrix} \frac{mg}{L}\omega_L\left(y - y_L\right) + \frac{1}{L}\tau_L \\ mg\omega_L \\ \tau_L \end{pmatrix} \tag{8}$$

and similarly for the right foot forces. Notice, of course, that $F_{LY} + F_{RY} = m\ddot{y}$ and $F_{LZ} + F_{RZ} = mg$.

Additionally, we impose the constraint that the center of pressure remain beneath the foot,

$$\begin{cases} |\tau_L| & \leq & F_{LZ}d \\ |\tau_R| & \leq & F_{RZ}d \end{cases} \tag{9}$$

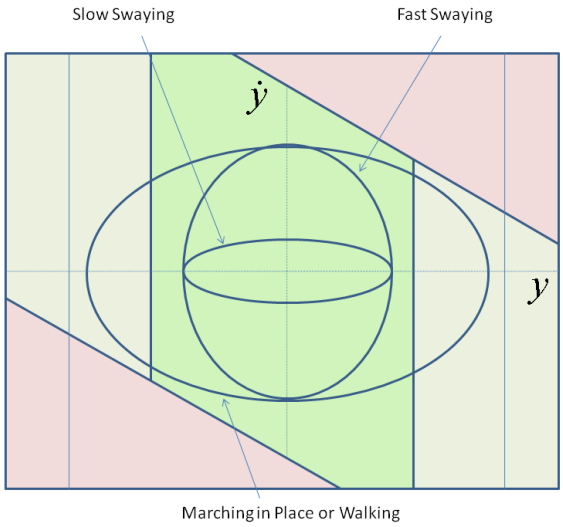

Fig. 4. Different energy profiles define different behaviors in the phase space of the center of mass.

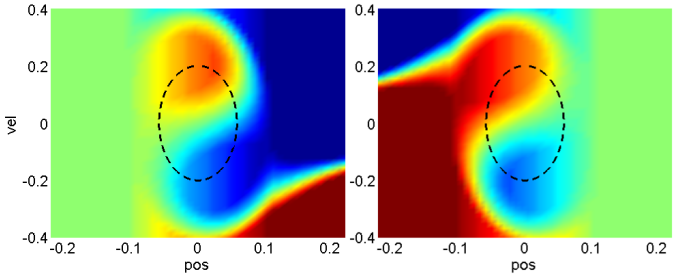

Fig. 5. The energy controller defines continuous nonlinear torque policies for the two ankles

By inserting Eq.(8) into Eq.(9), we get

$$\begin{cases} |\tau_L| & \leq & \omega_L mgd \\ |\tau_R| & \leq & \omega_R mgd \end{cases} \tag{10}$$

Notice that we can also write the constraint,

$$|\tau_L + \tau_R| \leq mgd. \tag{11}$$

We can also write constraints on the friction cone, which specifies that $F_Y < \mu F_Z$, where μ is a coefficient of friction, or

$$\omega_L \left(-L\mu - y + y_L\right) \leq \frac{\tau_L}{mg} \leq \omega_L \left(L\mu - y + y_L\right) \tag{12}$$

These constraints are illustrated in Figure 3. The amount of overlap between the friction constraints and center of pressure constraints depends on the coefficient of friction and the width of the foot. As the width of the foot increases, the maximum torque allowed by the center of pressure constraints increases, but the friction constraints remain the same. This suggests that the friction constraints are less important in the lateral direction, where the foot width is smaller, than in the sagittal direction where the foot length is larger.

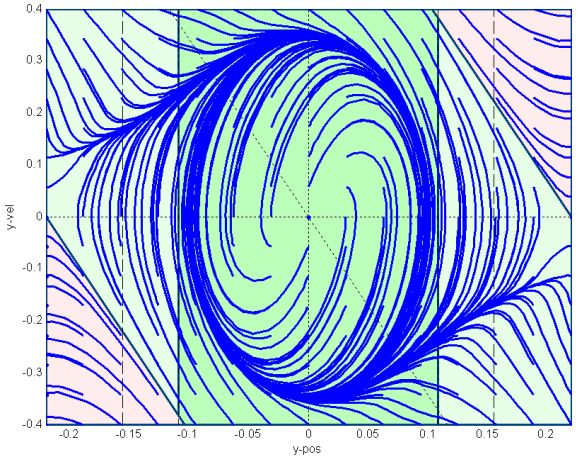

Fig. 6. Controlling the energy in the coronal plane causes the system to converge to a limit cycle

III. Orbital Energy Control

We have borrowed the idea of orbital energy to generalize control for balancing at a point as well as to a cycle. Zero energy corresponds to regulating to a point while non-zero energy corresponds to a cyclic motion. We define coronal energy with the ellipse,

$$E = a^2 \frac{\tilde{y}^2}{2} + b^2 \frac{\dot{y}^2}{2}, \tag{13}$$

defined in the phase space of the center of mass. This ellipse follows the trajectory,

$$y(t) = \frac{\sqrt{2E_d}}{a} sin\left(\frac{a}{b}t\right) \tag{14}$$

which gives the oscillation a frequency of

$$f = \frac{a}{2\pi b}. \tag{15}$$

Figure 4 illustrates various behaviors that can be represented by orbital energy. Our objective is to control the energy of the system. We achieve this by defining a Lyapunov function of the form,

$$V = \frac{1}{2}\left(E_d - E\right)^2 \tag{16}$$

The time derivative of Eq.(16) is

$$\dot{V} = -\left(b^2\ddot{y} + a^2\tilde{y}\right)\dot{y}\left(E_d - E\right) \tag{17}$$

In order to make $\dot{V} \leq 0$, we choose

$$\ddot{y}_{\text{des}} = -\frac{a^2}{b^2}\tilde{y} + K\dot{y}\left(E_d - E\right) \tag{18}$$

where K defines the rate of convergence to the desired energy. Using Eq.(5), we can write the inverse dynamics,

$$u = mL\left(-\frac{a^2}{b^2}\tilde{y} + \frac{g}{L}\alpha\tilde{y} + K\dot{y}\left(E_d - E\right)\right) \tag{19}$$

where $u = \tau_L + \tau_R$. The remaining task is to decide how to distribute the control between τ_L and τ_R while satisfying

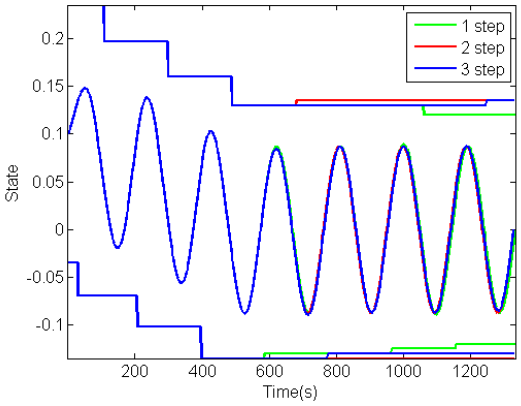

Fig. 7. Simulated trajectories using an N-step controller for 1, 2, and 3 step lookahead.

Eq.(10). A simple answer is to weight the torques linearly using

$$\begin{cases} \tau_L &= \omega_L u \\ \tau_R &= \omega_R u \end{cases} \tag{20}$$

The resulting control policies are shown in Figure 5 and example trajectories are shown in Figure 6.

IV. Stepping Control

Given an orbital energy controller that allows us to regulate the motion of the center of mass of the system, we propose an additional controller that decides where to step. Stepping can make use of knowledge of the future, as several steps are often required to bring the system back to a stable state. In addition, during a walking gait like the one defined by the orbital energy controller above, the steps should return the system to the original location after a large perturbation.

The pre-defined double support region, as described above, eliminates the decision of when to pick up or place the swing foot. Instead, as we leave the double support region, we only decide how far to move the swing leg. This determines the rest of the trajectory until the next single support phase when we can move the other swing leg. Because of this structure, we can write an N-step lookahead controller that considers a set of step distances from the current state and chooses the next step distance as the distance that minimizes an objective function of the form,

$$f = \sum_i k_1(E(X_i)-E_d)^2+k_2(W(X_f)-W_d)^2+k_3(X_f-X_d)^2, \tag{21}$$

where X_i are the states of the resulting trajectory, X_f is the final state, W_d is the desired stance width and X_d is a desired state. $E(X)$ and $W(X)$ represent the energy and step width, respectively, of the state X. The first term returns the system to the desired orbital energy, the second drives the stance width back to the desired stance width, and the third can be used to regulate the position of the system. The gains, k_i, are chosen by the user. Example trajectories using this controller can be seen in Figure 7.

TABLE I
Comparison of N-Step Controllers

Controller	Fall Percentage	Normalized Cost
1-step	5.6%	1.0
2-step	1.8%	0.9266
3-step	1.7%	0.9230

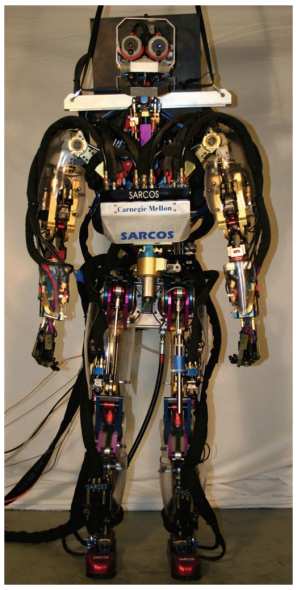

Fig. 8. Sarcos Humanoid robot

We compare the performance of 1, 2 and 3-step lookahead controllers in Table I. 1000 random initial states and desired energies were used to generate this data. Our results indicate that it is more reliable to perform a 2-step lookahead.

V. Humanoid Robot Control

Using the energy and stepping controllers developed for the Linear Biped Model, we can control our humanoid robot to perform similar tasks. Our humanoid robot, shown in Figure 8 uses hydraulic actuators at each joint with potentiometers to measure joint angles and load sensors to measure actuator force. After compensating for the viscous damping of the hydraulic actuators [19], we control the torque at each of the joints. The robot has 33 degrees of freedom (not including eyes, mouth and fingers). For the purposes of this paper, we only control the 14 joints of the lower body (7 joints in each leg).

A. Estimating Center of Mass

We can generalize our models to more complex systems, such as our humanoid robot. To do this we need to accurately estimate the state of the center of mass. We combine several sensors (joint potentiometers, accelerometers and feet force-torque sensors) and our simple model to give us an improved estimate of center of mass motion, as shown in Figure 9. Using the Linear Biped Model, we can use a Kalman Filter to combine these measurements. Our sensors give us one position

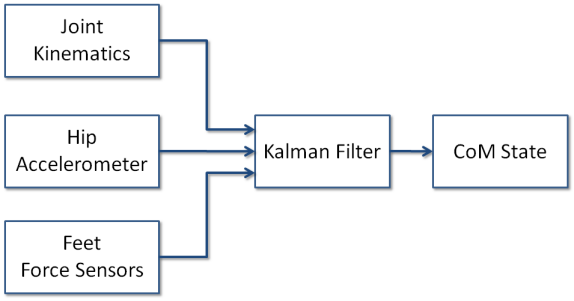

Fig. 9. Multiple measurements are combined using a Kalman filter to get improved center of mass state estimates.

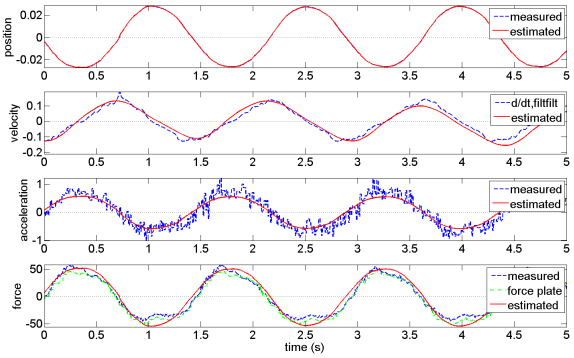

Fig. 10. A Kalman Filter using the LiBM gives smoother estimates of the position, velocity and acceleration of the center of mass.

measurement from the potentiometers and kinematics and two acceleration measurements from an accelerometer attached to the hip and the force sensors on the feet.

The process model is just the linear forward dynamics defined by Eq.(1) and Eq.(2), which can be written in state space form as

$$\begin{pmatrix} \dot{y} \\ \ddot{y} \end{pmatrix} = \begin{bmatrix} 0 & 1 \\ -\frac{g}{L}\alpha & 0 \end{bmatrix} \begin{pmatrix} y \\ \dot{y} \end{pmatrix} + \begin{bmatrix} 0 \\ \frac{1}{mL} \end{bmatrix} u \qquad (22)$$

The sensor model, however, becomes

$$z = \begin{bmatrix} 1 & 0 \\ -\frac{g}{L}\alpha & 0 \\ -\frac{mg}{L}\alpha & 0 \end{bmatrix} \begin{pmatrix} y \\ \dot{y} \end{pmatrix} + \begin{bmatrix} 0 \\ \frac{1}{mL} \\ \frac{1}{L} \end{bmatrix} u \qquad (23)$$

We discretize this model for our robot, which runs in a 1kHz control loop. Using a Kalman filter, we can combine these measurements to give us smooth position and improved velocity and force estimates, as shown in Figure 10.

B. Feedforward Control

The LiBM can be used to generate feedforward controls for the humanoid robot. Eq.(8) predicts the forces at the feet needed to perform energy control. We control the robot by trying to re-create these forces.

Let $J_R(q)$ and $J_L(q)$ be the Jacobian from the middle of the feet to the center of mass, as shown in Figure 11. We use the feet force sensors to detect when the feet are on the ground, in which case we treat each leg as a manipulator attached to

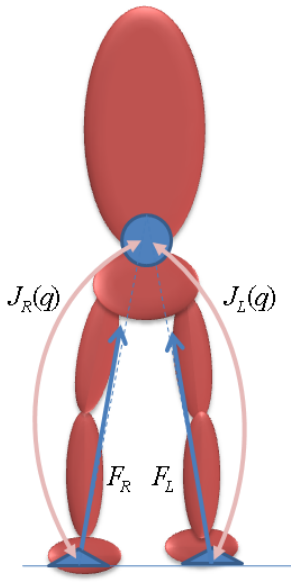

Fig. 11. The Jacobian from the center of mass to each foot relates the LiBM to the humanoid robot. We treat the upper body as a lumped mass.

the ground. To control the robot, we apply a controls to the joints of the left and right leg of the form,

$$\tau_L = J_L^T(q) f_L + \tau_L^{pd} \qquad (24)$$

$$\tau_R = J_R^T(q) f_R + \tau_R^{pd} \qquad (25)$$

where f_L and f_R are found using Eq.(8) and τ_L^{pd} and τ_R^{pd} are low-gain PD controllers that correspond to a desired home pose and zero velocity.

VI. Results and Discussion

In this paper, we defined energy as an ellipse in the phase plane of the center of mass in Eq.(13). We are not limited to elliptical energy profiles. Other parametric curves could be used to customize behaviors or optimize for control effort. We have has explored non-parametric representations, such as optimal trajectories found through dynamic programming. However, these solutions are sometimes difficult to compute and generally have to be recalculated for different parameters, such as desired energy or double support ratio.

Stepping control was achieved through a lookahead procedure that only considers the size of the next few steps. While we were able to achieve a lower cost by looking ahead more steps, the improvement was small. A one-step lookahead can be performed very quickly and was still able to recover about 95% of the time. It is unclear whether additional lookahead is worth the additional computation time. For this reason, we attempted to fit a linear policy to approximate the 2-step lookahead while only calculating the 1-step lookahead. This proved to be difficult and did not result in better performance.

We have performed a variety of experiments on our Sarcos robot using the methods described in this paper. We are currently able to march in place, lifting the feet slightly off the ground. The center of mass is controlled to achieve a desired

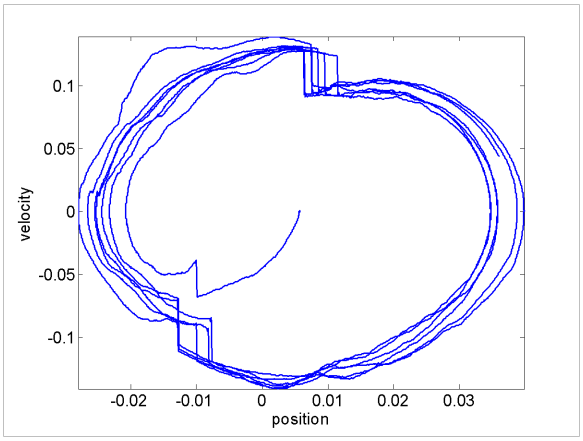

Fig. 12. Robot center of mass trajectory while marching in place

energy profile, as shown in Figure 12. We have also explored a variety of center of mass filter formulations which can be used not only to estimate state, but estimate other parameters such as offsets, model parameters and external pushes.

Pushing and step recovery are the primary focus of our research. Figure 13 shows a push experiment where the robot was marching in place and then pushed to the side. It took two steps while controlling itself to return to a desired stance width and remained balanced.

The mapping of the controls from the simple LiBM to the full robot can be improved in a variety of ways. In particular, using a rigid body dynamics model of the robot, we can use inverse dynamics to achieve desired reaction forces or, equivalently, center of mass accelerations. Such calculations can be performed efficiently online [11] [20], but rely heavily on an accurate model and robot calibration.

Future work will focus on applying robust control techniques to the LiBM and then transferring this robustness to the humanoid robot. It is our hope that this type of controller design technique will simplify the often brittle and tedious design of humanoid robot controllers.

VII. Conclusion

The Linear Biped Model has been used to study a wide range of humanoid behaviors, including balance and step recovery. The energy controller we derived is useful for stabilizing the robot during these often periodic activities. Future work is focusing on a 3D version of the LiBM, which can be used for walking and also step recovery of pushes in all directions.

References

[1] S. Kajita and K. Tani, "Study of dynamic biped locomotion on rugged terrain-derivation andapplication of the linear inverted pendulum mode," in *Proceedings of the IEEE International Conference on Robotics and Automation*, vol. 2, April 1991, pp. 1405–1411.

[2] S. Kajita, T. Yamaura, and A. Kobayashi, "Dynamic walking control of a biped robot along a potential energy conserving orbit," *IEEE Transactions on Robotics and Automation*, vol. 8, no. 4, pp. 431–438, Aug 1992.

[3] S. Kajita, F. Kanehiro, K. Kaneko, K. Fujiwara, K. Harada, K. Yokoi, and H. Hirukawa, "Biped walking pattern generation by using preview control of zero-moment point," in *Proceedings fo the 2003 IEEE International Conference on Robotics and Automation*, Taipei, Taiwan, September 2003, pp. 1620–1626.

[4] J. Chestnutt, M. Lau, K. M. Cheung, J. Kuffner, J. K. Hodgins, and T. Kanade, "Footstep planning for the honda asimo humanoid," in *Proceedings of the IEEE International Conference on Robotics and Automation*, April 2005.

[5] J. Pratt and R. Tedrake, "Velocity based stability margins for fast bipedal walking," in *First Ruperto Carola Symposium in the International Science Forum of the University of Heidelberg entitled "Fast Motions in Biomechanics and Robots"*. Heidelberg Germany: Springer Berlin / Heidelberg, September 7-9 2005.

[6] B. Stephens, "Humanoid push recovery," in *Proceedings of the IEEE-RAS International Conference on Humanoid Robots*, 2007.

[7] S.-H. Lee and A. Goswami, "Reaction mass pendulum (rmp): An explicit model for centroidal angular momentum of humanoid robots," in *IEEE International Conference on Robotics and Automation*, April 2007, pp. 4667–4672.

[8] B. Stephens, "Integral control of humanoid balance," in *Proceedings of the IEEE/RSJ 2007 International Conference on Intelligent Robots and Systems*, 2007.

[9] C. Atkeson and B. Stephens, "Multiple balance strategies from one optimization criterion," in *The IEEE-RAS 2007 International Conference on Humanoid Robots*, 2007.

[10] L. Sentis and O. Khatib, "A whole-body control framework for humanoids operating in human environments," in *Proceedings 2006 IEEE International Conference on Robotics and Automation*, 2006, pp. 2641–2648.

[11] S.-H. Hyon, J. Hale, and G. Cheng, "Full-body compliant humanhumanoid interaction: Balancing in the presence of unknown external forces," *IEEE Transactions on Robotics*, vol. 23, no. 5, pp. 884–898, October 2007.

[12] J. Pratt, J. Carff, S. Drakunov, and A. Goswami, "Capture point: A step toward humanoid push recovery," in *6th IEEE-RAS International Conference on Humanoid Robots*, December 2006, pp. 200–207.

[13] J. Rebula, F. Canas, J. Pratt, and A. Goswami, "Learning capture points for bipedal push recovery," in *Proceedings of the IEEE International Conference on Robotics and Automation*, 2008, pp. 1774–1774.

[14] S. Ramamoorthy and B. Kuipers, "Trajectory generation for dynamic bipedal walking through qualitative model based manifold learning," in *Proceedings of the IEEE International Conference on Robotics and Automation*, 2008, pp. 359–366.

[15] Y. Abe, C. K. Liu, and Z. Popovic, "Momentum-based parameterization of dynamic character motion," *ACM SIGGRAPH / Eurographics Symposium on Computer Animation*, pp. 194–211, 2004.

[16] K. Yin, D. K. Pai, and M. van de Panne, "Data-driven interactive balancing behaviors," *Pacific Graphics*, Oct 12-14 2005.

[17] D. Choi, C. Atkeson, S. J. Cho, and J.-Y. Kim, "Phase plane control of a humanoid," in *8th IEEE-RAS International Conference on Humanoid Robots*, Dec 2008, pp. 145–150.

[18] A. Kuo, "Stabilization of lateral motion in passive dynamic walking," *International Journal of Robotics Research*, vol. 18, no. 9, pp. 917–930, 1999.

[19] D. C. Bentivegna, C. G. Atkeson, and J.-Y. Kim, "Compliant control of a hydraulic humanoid joint," in *IEEE Conference on Humanoids*, 2007.

[20] M. Mistry, J. Nakanishi, G. Cheng, and S. Schaal, "Inverse kinematics with floating base and constraints for full body humanoid robot control," in *Proceedings of the IEEE-RAS International Conference on Humanoid Robots*, 2008, pp. 22–27.

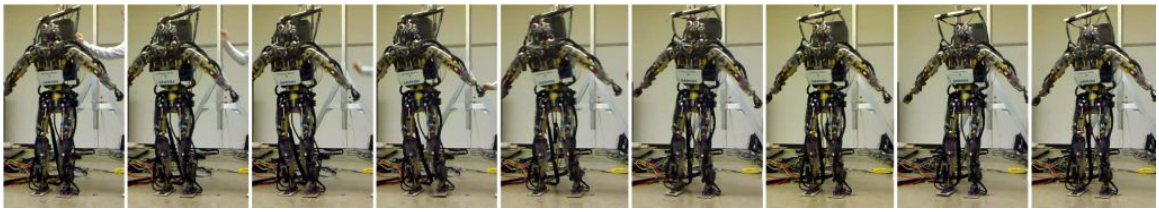

Fig. 13. While marching in place, the robot is pushed, takes a step to maintain its stance width and recovers. See more videos at http://www.youtube.com/humanoidbalance